Indian Journal of Chemistry
Vol. 57A, March 2018, pp. 435-443

Synthesis, characterization, luminescence and photocatalytic studies of layered perovskites $NaMMgWO_6$ (M = La, Pr, Sm)

Sreenu K, Gundeboina Ravi, CH Sudhakar Reddy, Ravinder Guje & M Vithal*

Department of Chemistry, Osmania University, Hyderabad 500 007, Telangana, India

Email: muga_vithal@osmania.ac.in

The synthesis, characterization, optical and photocatalytic studies of *AA'BB'*X_6 type perovskites, $NaMMgWO_6$ (M = La, Pr, Sm), which have an ordering of both the cation sub-lattices, is reported. The obtained $NaMMgWO_6$ materials have been prepared using ethylene glycol assisted gel-burning method and characterized by X-ray diffraction patterns, UV-vis diffused reflectance spectra, scanning electron microscopy, Fourier transformation infrared spectra, energy dispersive spectra and fluorescence spectra. The photocatalytic dye degradation performance of the as-synthesized perovskites has been evaluated with methylene blue and methyl violet as model water pollutants using radical quenchers.

Keywords: Perovskites, Layered perovskites, Photocatalytic activity, Photoluminescence, Chromaticity, X-ray diffraction, Band gap energy, Gel burning method

During the past several decades, the contamination of water bodies (lakes, rivers and ponds, etc.) has been treated as a major environmental problem. The textile industry produces a large volume of wastewater, which if not treated properly, can cause serious environmental contamination due to its toxicity and carcinogenicity that can be harmful to human health, aquatic lives and environment.[1-4] To resolve this problem, various methods such as biodegradation, coagulation, adsorption, advanced oxidation processes (AOP) and the membrane process have been suggested.[5-7] All these processes have some advantages or disadvantages over the other methods. A balanced approach is therefore needed to look into the worthiness on choosing an appropriate method, which can be used to degrade the dye. Among these techniques, the advanced oxidation process appears to be a most promising method. The semiconductor based photocatalysis, one of the AOPs, is found to be effective in removing dyes from water, without generating any secondary toxic compounds.[8-10]

Semiconductor metal oxides with the perovskite structure have long attracted the interest of chemists due to the significant spectrum of their properties. The properties and applications of perovskites are directly associated with their electronic structures. These oxides show ferroelectricity,[11] colossal magnetoresistance,[12] itinerant electron ferromagnetism,[13] multiferroic behavior,[14] piezoelectricity,[15] and superconductivity.[16] The perovskite structure with high-symmetry (cubic symmetry belongs to space group *Pm*-3*m*)) of general composition, ABX_3, can be described as a three-dimensional array of corner sharing BX_6 octahedra with the A-site cations occupying the 12 coordinate cubo-octahedral cavities that are formed between any eight such BX_6 units.[17] The structure is flexible for substitutions at both cations and anions, giving rise to a large number of compounds. However, chemical substitutions at the cation sites can modify the symmetry and properties of cubic perovskites. A random or an ordered structural arrangement takes place on replacement of multiple cations at either the A-site or the B-site. These structural arrangements depend on the size and charge difference of cations. A larger difference in size and charge of cations favor ordered arrangement, whereas cations that are comparable in size and charge tend to be randomly distributed.[18]

Further, the composition and ordered arrangement of perovskite vary with the substitutional site. For example, B-site substitution with two cations in 1:1 ratio leads to perovskites in a rock salt ordering with the composition, $A_2BB'X_6$. Perovskites with rock salt ordering (i.e., ordering of B site) is very common and has been studied widely.[19,20] The A-site cation ordering prefers the layered arrangement and is observed in anion deficient perovskites with the general formula, $AA'B_2X_5$.[21,22] Furthermore, the perovskites that have an ordering of both the cation sub-lattices $AA'BB'X_6$ ($NaLnMgWO_6$), i.e., rock salt

ordering of B-site cations and a layered ordering of A site cations, are quite rare. Sekiya *et al.*[23] first reported the perovskite of composition, $NaLaMgWO_6$, by solid state method at 1100 °C with an ordering of the Na and La-cations and a rock salt ordering of the Mg and W-cations. Later, some perovskites with similar structures have been reported.[24-28] However, studies on the catalytic properties of double perovskites are scanty.[29,30] It has also been reported that a few W containing double perovskites are chemically unstable and not suitable for photocatalysis.[30] Subsequently, King *et al.*[31] prepared fourteen new double perovskite materials with the compositions, $NaLnMnWO_6$ (Ln = Ce, Pr, Sm, Gd, Dy, Ho) and $NaLnMgWO_6$ (Ln = Ce, Pr, Sm, Eu, Gd, Tb, Dy, Ho) by the solid state method. These samples were calcined in the temperature range of 900–950 °C. Recently, Eu^{3+}-doped $NaLaMgWO_6$ ($NaLa_{1-x}Eu_xMgWO_6$, x = 0.05, 0.1, 0.3, 0.5, 0.7, 0.9, 1) is reported to have been prepared by sol-gel method at 1100 °C for 6 h.[32]

In view of the above, we thought it worthwhile to prepare W containing double perovskites and study their photocatalytic properties and chemical stability. Herein, layer type materials with an ordering of A site cations Na/M (M= La, Pr, Sm) and rock salt ordering of B-site cations Mg/W of compositions $NaLaMgWO_6$ (NLMW), $NaPrMgWO_6$ (NPMW) and $NaSmMgWO_6$ (NSMW) were prepared by gel burning method. These materials were taken as model catalysts to degrade the organic pollutants. The photocatalytic activity of NLMW, NPMW and NSMW over methylene blue (MB) and methyl violet (MV) are presented. The chemical stability of these materials after photocatalysis is also studied.

Materials and Methods

Synthesis and characterization

Polycrystalline powders of compositions, $NaLaMgWO_6$, $NaPrMgWO_6$ and $NaSmMgWO_6$, were synthesized by gel burning method. The following analytical grade chemicals were used as received without further purification: $NaNO_3$, La_2O_3, Sm_2O_3, Pr_6O_{11}, HNO_3, $Mg(NO_3)_2$, W powder, H_2O_2, citric acid and ethylene glycol Stoichiometric amounts of all the reagents in their soluble state (viz., $Mg(NO_3)_2$ and $NaNO_3$ in water, Ln_2O_3 in HNO_3 solution to form $Ln(NO_3)_3$ and tungsten powder in H_2O_2 solution) were mixed and stirred for 2 h. Citric acid was then added to this mixture in the mole ratio of 1:2. The resultant homogenous metal citrate solution was heated at 100 °C until the solution was reduced to half of its original volume. Now, ethylene glycol, a gelating agent, was added in the mole ratio of 1:1.2 (metal citrate: ethylene glycol) and subsequently the temperature was raised to 160 °C. After a few hours, a black porous solid was obtained. It was crushed to a fine powder and heated isothermally at 700 °C for 6 h in a muffle furnace and cooled naturally to room temperature.

The phase identification of the materials was examined by powder X-ray diffraction (PXRD) data using Cu-Kα radiation (λ = 1.5406 Å, Rigaku Miniflex-600, 40 kV, 20 mA). The PXRD patterns were obtained at room temperature using the fixed time mode over an angular step size of 2θ = 0.02° and scan step time of 0.15 s in the 2θ range 5–80°. Rietveld analysis of a PXRD pattern was performed to refine the crystal structure. Fullprof.2k. program was used for the structural refinement with a pseudo-Voigt peak-shape function as a profile function. FT-IR spectral analysis was made on a Shimadzu spectrometer using KBr pellets. The SEM-EDS images were taken on a Hitachi SU-1500 variable pressure scanning electron microscope. The UV-vis diffuse reflectance spectra (UV-vis DRS) of the samples were recorded using Jasco V-650 UV-vis spectrophotometer and $BaSO_4$ was used as a reference material. Reflectance spectra were recorded in the wavelength range 700–200 nm and the reflectance was transformed into the Kubelka-Munk function. Photon energy at the absorption edge was estimated by extrapolating the linearly ascending portion of the spectrum to the x-axis, and the value was defined as an optical bandgap. The photoluminescence (PL) spectra were recorded using a Jasco FP-8500 spectrofluorometer. Interactive CIE software (CIE coordinate calculator) was used to identify the color coordinates of the phosphors.

Photocatalytic activity

The photocatalytic activity of as-synthesized catalysts was tested using Heber visible annular type photoreactor equipped with a 300 W tungsten lamp (wavelength range 380–840 nm). In the experiment, 50 mL of 10^{-5} M aqueous MB (or MV) solution comprising of 50 mg catalyst ($NaMMgWO_6$ (M = La, Pr and Sm)) was aerated in darkness for 60 min to achieve the adsorption-desorption equilibrium. Then, the resultant solution was illuminated by a 300 W tungsten lamp and aliquots of the aqueous dye solution were collected at regular 30 min intervals.

The absorbance of illuminated dye samples was recorded using a spectrophotometer. The MB (or MV) degradation efficacy has been determined as follows: Degradation(%) = $\{(A_0–A_t)/A_0\}\times100$, where A_0 and A_t are the absorbance of MB (or MV) solution before and after photoirradiation with a UV-vis spectrophotometer.

Radical (most reactive species in the photocatalytic process) quenching tests were carried out to study the MB (or MV) dye degradation mechanistic pathway. In this experiment, isopropyl alcohol (IPA), ammonium oxalate (AO) and benzoquinone (BQ) are used to quench the hydroxyl ($^{\bullet}OH$) radicals, holes (h^+) and superoxide ($O_2^{\bullet-}$) radicals respectively. The individual radical effect on dye degradation was studied. For this 2 mL of 2 mM quencher was added to 50 mL of aqueous dye solution under identical experimental conditions. The dye degradation during this process was determined as discussed above.

The production of $^{\bullet}OH$ radicals during the photocatalytic reaction was further substantiated by the terephthalic acid experiment. Typically, 50 mg of sample was suspended in 50 mL of a 0.02 mol L^{-1} NaOH solution containing 20 mg of terephthalic acid (TA). The suspension was illuminated under visible light (300 W tungsten lamp) and 3–5 mL of the resultant solution was collected at regular 30 min intervals. The fluorescence spectra of these samples were recorded on a Shimadzu RF-5301PC fluorescence spectrophotometer at the fixed excitation wavelength of 320 nm.

Reusability and stability

To test the reusability and stability of the catalysts, the catalyst was collected after the first cycle of the photocatalytic experiment, washed with distilled water to remove adsorbed dye molecules and subjected to the second cycle of photodegradation. This procedure was repeated for the third cycle of photodegradation.

Results and Discussion

All the compositions investigated were prepared by ethylene glycol assisted gel-burning method. To the best of our knowledge, $NaMMgWO_6$ (M = La, Pr, Sm) has been prepared by sol-gel method at low temperature (700 °C) with W metal powder as the tungsten source for the first time. For the phase identification, these powder samples were subjected to PXRD measurements. The PXRD patterns of these compositions are shown in Fig. 1. All the powder patterns are similar to each other, free from impurities and consistent with diffraction pattern expected for double perovskites (JCPDF: 88-1761). The observation of lower width for base line indicates crystalline nature and absence of any amorphous phase. The *d*-lines of these patterns, when plotted in the expanded scale, show a small shift in the position (inset Fig. 1) resulting from the change in unit cell parameter. A shift of *d*- line towards higher 2θ values leads to a decrease in unit cell parameter (and hence unit cell volume).[33] Here, the systematic shift of *d*- lines can be attributed to the ionic size of La^{3+} (1.032 Å), Pr^{3+} (0.99 Å) and Sm^{3+} (0.96 Å).[34] The structural analysis was carried out by Rietveld refinements (Fullprof.2k). The Rietveld structure refinements revealed that all the samples crystallize in monoclinic system with $P2_1(4)$ space group (See Fig. S1 and Table S1, Supplementary Data). The obtained lattice parameters are comparable with the reported values.[23,25]

The morphologies of NLMW, NSMW and NPMW were obtained from scanning electron microscopy. All the samples have irregular morphology with significant agglomeration (Supplementary Data, Fig. S2(a-c). The X-ray energy dispersion spectra of NLMW, NSMW and NPMW perovskites are shown in Fig. S2 (d-f) (Supplementary Data). The stoichiometric composition analyses of these perovskites were obtained by their X-ray energy dispersion spectra. The atomic ratio of Na, M, Mg and W in NLMW, NSMW and NPMW samples was found to be approximately 1:1:1:1 and confirms the

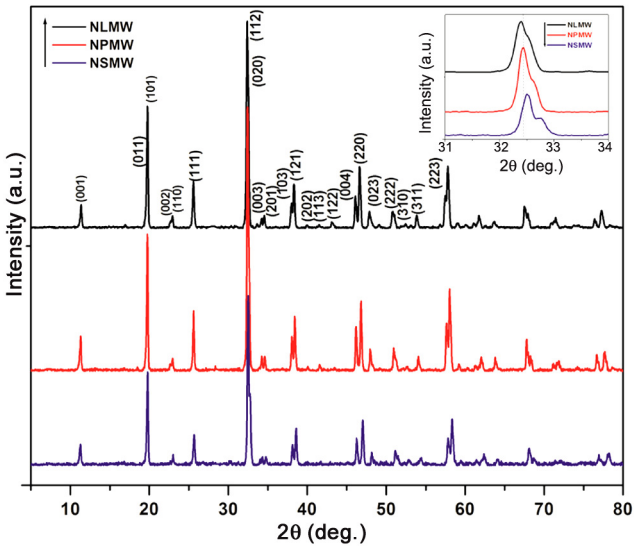

Fig. 1 – Powder XRD patterns of NLMW, NSMW and NPMW. [Inset shows the shift of *d*-lines].

stoichiometric composition of NLMW, NSMW and NPMW as $NaLaMgWO_6$, $NaSmMgWO_6$, and $NaPrMgWO_6$ respectively.

The FT-IR spectra of all compositions were recorded in the range 300-4000 cm^{-1} to ascertain the solid solution phase and the local symmetry of the perovskite oxides. The FT-IR-spectra of NLMW, NPMW and NSMW in the 300–1000 cm^{-1} range are similar to each other except in their band positions (Supplementary Data, Fig. S3). From the observed bands of these samples, it is evident that local symmetry of these oxides is akin to those reported by Sekiya *et al*.[23] The two strong and broad bands at 350–450 and 650–720 cm^{-1} are assigned to the internal modes of octahedral, while two strong bands located at 820 and 870 cm^{-1} are due to B-O stretching mode. It is reported that the bands at 820 and 870 cm^{-1} are absent in double perovskites crystallized in cubic symmetry with undistorted BO_6 octahedra. Their presence in the NLMW, NPMW and NSMW may be due to the monoclinic distortion from cubic symmetry having distorted BO_6 octahedra.[35] The observed regular right shift of vibrational bands from NLMW to NSMW towards lower wave number can be ascribed to higher ionic radius of La^{3+} as compared to Sm^{3+} (Fig. S3). The higher ionic radius can lead to the decrease in force constant, which can cause a decrease in its vibrational frequency.[36]

Since the properties and applications of perovskites are directly associated with their electronic structures, to identify their potential applications an understanding of the electronic properties is required. UV-visible absorbance spectra of NLMW, NPMW and NSMW are recorded in the region 200–700 nm (Fig. 2). It is observed that the absorption edges of NLMW, NPMW and NSMW were found to be around 500 nm, 448 nm and 400 nm respectively. The shapes of absorption edges of all the three compounds are steep. Further, the absorption spectrum (DRS) of NPMW is characterized by four bands designated as I, II, III and IV belonging to Pr^{3+}, while NSMW is characterized by three bands designated as A, B and C belonging to Sm^{3+}. In the DRS of NPMW, the observed bands at 453, 478, 486 and 595 nm are assigned to transitions from $^3H_4 \rightarrow {}^3P_2$ (I), $^3P_1$ (II), $^3P_0$ (III) and $^1D_2$ (IV) respectively of Pr^{3+} ion (Fig. 2b). The bands at 407, 479 and 560 nm, in the DRS of NSMW, is assigned to the transitions $^6H_{5/2} \rightarrow {}^6P_{3/2}$ (A), $^4G_{7/2}$ (B) and $^4G_{5/2}$ (C) respectively of Sm^{3+} ion (Fig. 2c). The observed wavelengths and wave numbers of the bands along with their assignments are given in Table S2 (Supplementary Data). The band gap energy of NLMW, NPMW and NSMW was calculated from the absorption spectra by using the Kubelka-Munk (KM) method, (Supplementary Data, Fig. S4).[33] The extrapolation of the linear portion of KM function versus photon energy plot on to the *x*-axis gives the band gap energy. It is found to be 2.47, 2.76 and 3.1 eV for NLMW, NPMW and NSMW respectively. However, previous reports revealed that the band gap energy of $NaLaMgWO_6$ is~4 eV.[32,37] The literature on tungstate double perovskites strongly indicates that band gap in the approximate range of 3.3–4.0 eV is expected for these compounds. In the present investigation, this discrepancy can be explained as follows: In general, the bandgap energy (E_g) of the semiconductor material is related to its band edge position. The relative shift of the absorption edge of the semiconductor depends strongly on the (i) method of preparation and (ii) difference between the ionic radius of the dopant and the host cations as well as on the chemical nature of the dopants. It is likely that the low temperature sol gel route creates some defects that stretch the absorption tail into the visible light region, leading to lower bandgap energy.

The rare earth ion containing materials can act as phosphor materials because of their photoabsorption and emission properties. Phosphors can be used in a variety of display applications, such as electroluminescent, photoluminescent, plasma and field emission displays, LCDs, X-ray detectors, cathode ray tubes (CRTs), LEDs and many more.[38,39]

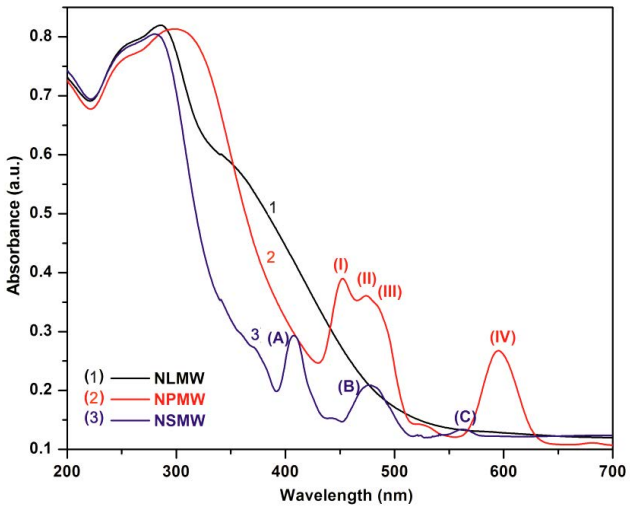

Fig. 2 – Absorbance spectra of NLMW (1), NSMW (2) and NPMW (3).

The significant factors for phosphor materials are its color point, the emission spectrum and the emission lifetime. It is also reported that $NaLaMgWO_6$ can act as host material for the rare earth ions and have great potential in solid state lighting.[32,40,41] However, the luminescence studies on the complete replacement of La in $NaLaMgWO_6$ by rare earth ion are not reported. Hence, an attempt was made to study photoluminescence and color points of NPMW and NSMW.

Room temperature excitation and emission spectra of NPMW and NSMW were recorded. Excitation and emission spectra of NPMW and NSMW are consistent with reported spectra.[42,43] Figure 3a shows the emission spectrum of NSMW under excitation at 450 nm. It is characterized by peaks at 565 nm, 605 nm, and 644 nm which are assigned to $^4G_{5/2}\rightarrow{}^6H_J$ (J = 5/2, 7/2, 9/2) transitions of Sm^{3+}. In Sm^{3+}, the electronic transition $^4G_{5/2}\rightarrow{}^6H_{5/2}$ is purely magnetic dipole (MD) transition while $^4G_{5/2}\rightarrow{}^6H_{7/2}$ transition is MD as well as electric dipole (ED) allowed and the other transition $^4G_{5/2}\rightarrow{}^6H_{9/2}$ is purely ED allowed transition. The excitation spectrum (λ_{em} =596 nm) of as prepared NSMW compound is shown in Fig. 3b Several excitation bands are observed and are assigned to the electronic transitions: $^6H_{5/2}\rightarrow{}^4H_{7/2}$ (365 nm), $^6H_{5/2}\rightarrow{}^6P_{7/2}$ at 378 nm, $^6H_{5/2}\rightarrow{}^4F_{7/2}$ at 405 nm, $^6H_{5/2}\rightarrow{}^6P_{5/2}$ at 419 nm, $^6H_{5/2}\rightarrow{}^4G_{9/2}$ at 444 nm, and $^6H_{5/2}\rightarrow{}^4I_{11/2}$ at 483 nm.

Figure 3c shows the emission spectrum of NPMW upon excitation at 450 nm. This spectrum is characterized by the bands that are assigned to the electronic transitions, $^3P_0\rightarrow{}^3H_6$ at 624 nm, $^3P_0\rightarrow{}^3F_2$ at

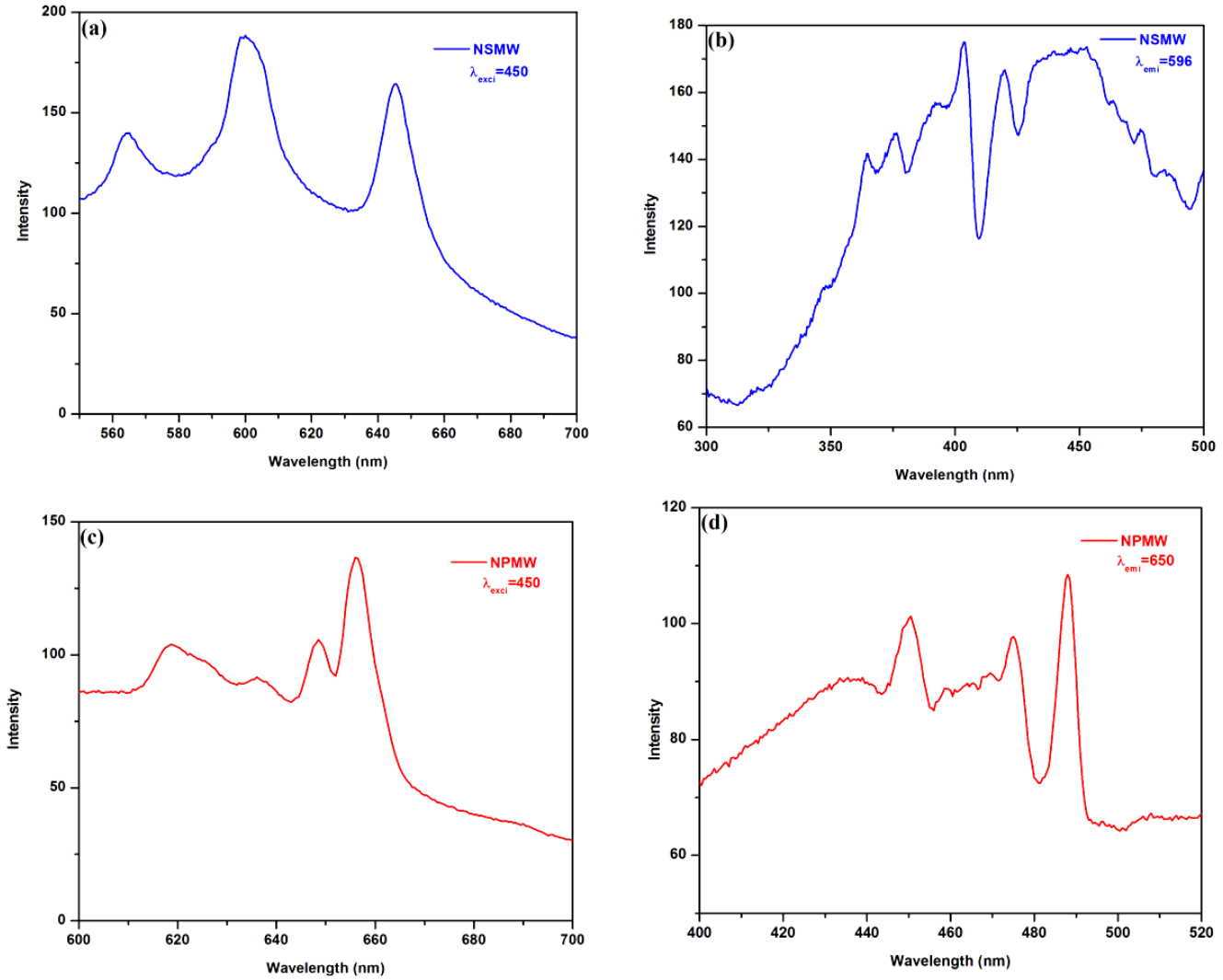

Fig. 3 – Excitation and emission spectrum of (a & b) NSMW and (c & d) NPMW.

650 nm and $^1D_2 \rightarrow {}^3H_5$ at 660 nm. The excitation spectrum of NPMW monitoring the emission at 650 nm is shown in Fig. 3d. It is characterized by absorption bands at 450, 475 and 489 nm that are assigned to *f-f* electronic transitions of Pr^{3+} ion, $^3H_4 \rightarrow {}^3P_2$, $^3H_4 \rightarrow {}^3P_1$, $^1I_6$ and $^3H_4 \rightarrow {}^3P_0$ respectively.

The color point of phosphors is defined according to the convention of the Commission Internationale d′Eclairge (CIE) diagram.[44] The CIE diagram is used to determine the color of the phosphor material. The color of any phosphor material or light source in color space is represented by color coordinates (x, y). The emission spectrum of the NPMW and NSMW phosphors was converted to the CIE 1931 chromaticity diagram using their photoluminescence data and CIE coordinate calculator. The color purity of a phosphor was calculated as:

$$\text{Colour purity} = \frac{\sqrt{(x-x_i)^2+(y-y_i)^2}}{\sqrt{(x_d-x_i)^2+(y_d-y_i)^2}} \times 100$$

, where (x, y) and (x_i, y_i) are the color coordinates of emission light and CIE white illuminate (0.33, 0.33) respectively and (x_d, y_d) are chromaticity coordinates of the dominant wavelength points. The CIE x–y color coordinate diagrams for the NPMW and NSMW are shown in Fig. S5 (Supplementary Data). The (x_d, y_d) values for NPMW and NSMW are found to be (0.439, 0.554) and (0.448, 0.544), respectively. The CIE color purity for the as-prepared samples, NPMW and NSMW, was found to be 94% and 95.9% respectively. Phosphor materials emit different colors, depending on the color purity of materials. Low and high color purity materials are used as sources of white light and monochromatic light, respectively. From the obtained color purity, NPMW and NSMW can be used in monochromatic light source materials.

Based on the bandgap energy calculations, the as-synthesized perovskite materials may be employed as visible light active photocatalysts. To compare the photocatalytic behavior of NLMW, NPMW and NSMW samples, the photocatalytic degradation of methylene blue (MB) as model contaminant was carried out under visible light irradiation. Figure 4a shows that 29% of MB was degraded without catalyst after 180 min. This is due to the self-photolysis of MB.[45] However, in the presence of NLMW, NPMW and NSMW catalysts, the MB degradation was about 94%, 88% and 86% (including photolysis of MB) respectively.

The photocatalytic behavior of NLMW, NPMW and NSMW materials, over methyl violet (MV) dye was also carried out under the similar conditions (Fig. 4b). The dye degradation was about 91%, 80% and 78% (including self-photolysis about 10 %) after 180 min visible light illumination respectively in the presence of NLMW, NPMW and NSMW. These results reveal that as-prepared NLMW, NPMW and NSMW are suitable and effective photocatalyst under visible light irradiation. It is obvious that, among these three photocatalysts, NLMW shows higher photocatalytic behavior than the other catalysts in the degradation of both the dyes. The reason for the

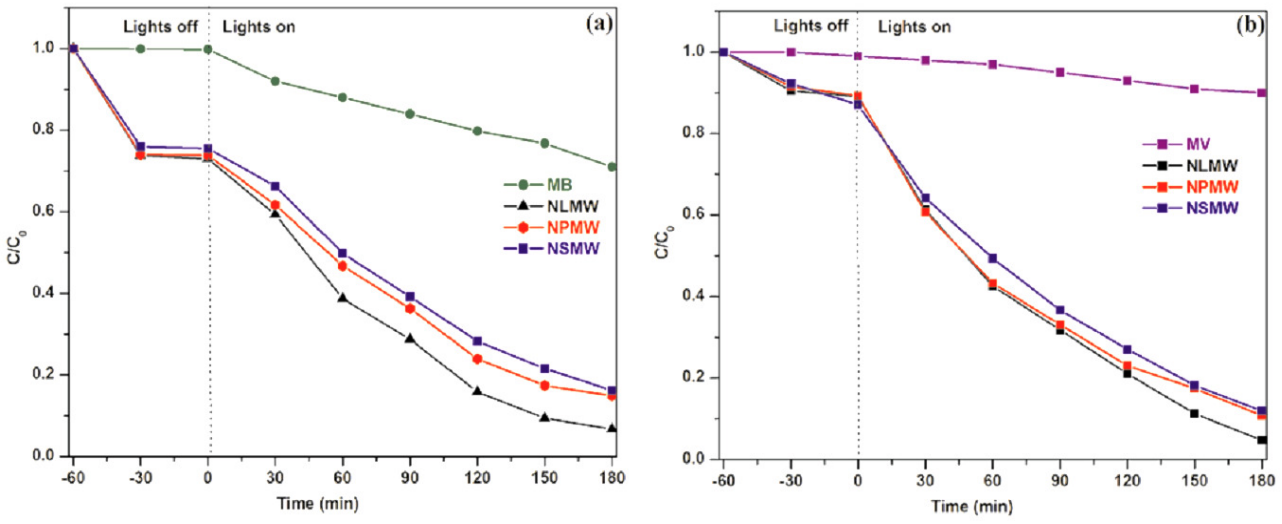

Fig. 4 – Degradation curves of (a) MB and (b) MV solutions under visible light irradiation in presence of NLMW, NSMW, and NPMW photocatalysts respectively.

higher photocatalytic efficiency of NLMW can be attributed to its lower bandgap energy compared to that of NPMW and NSMW. This statement is further supported from the terephthalic acid (TA) probe experiment.

The suggested mechanism of the photocatalytic degradation of MB (or MV) can be explained by Scheme 1.[45]

$$\text{Catalyst} + h\nu \rightarrow e^-_{CB} + h^+_{VB}$$
$$H_2O + h^+_{VB} \rightarrow OH^\bullet + H^+$$
$$O_2 + e^-_{CB} \rightarrow O_2^{\bullet -}$$
$$O_2^{\bullet -} + H^+ \rightarrow HO_2^\bullet$$
$$2HO_2^\bullet \rightarrow H_2O_2 + O_2$$
$$H_2O_2 \rightarrow 2OH^\bullet$$
$$HO_2^\bullet \text{ or } O_2^{\bullet -} \text{ or } OH^\bullet + \text{MB or MV} \rightarrow \text{Byproducts}$$

Scheme 1

The above mechanistic pathway of dye degradation shows that the holes (h^+), superoxide ($O_2^{\bullet -}$) and hydroxyl $^\bullet$OH radicals play key roles in the dye degradation process. Hence, in the present study, additional experiments were carried out to examine the roles of h^+, $O_2^{\bullet -}$ and $^\bullet$OH during the photoreaction. For this, we have studied the photodegradation of MV by quenching these reactive species with ammonium oxalate (AO), benzoquinone (BQ) and isopropyl alcohol (IPA) as quencher for quenching the holes (h^+), $O_2^{\bullet -}$ and $^\bullet$OH respectively during the photocatalytic reaction.[46-48] Figure 5a shows the results of MV photodegradation over NLMW in the presence of AO, BQ and IPA. It was observed that photocatalytic degradation percentage of MV was reduced from 91% to about 69%, 78% and 80%, respectively after the same time period in the presence of the quenchers, IPA, AO and BQ. Thus, the quenching studies reveal that h^+, $O_2^{\bullet -}$ and $^\bullet$OH radicals play an important role in the degradation of MV. However, the MV degradation was highly reduced by the quenching of h^+ (91% and 69% in the absence and presence of AO). It confirms that $^\bullet$OH radicals play a major role in the dye degradation process. It is known that the higher rate of formation of $^\bullet$OH radicals during the photoreaction leads to a higher photocatalytic activity.

As stated earlier, NLMW shows higher photocatalytic activity because of its lower band gap energy. The lower band gap energy of material leads to an increase in the number of the absorbed photons and produces a larger number of electron-hole pairs. Since the generated holes, which have escaped in the rapid carrier recombination process, react with surface water and form $^\bullet$OH radicals, it is believed that NLMW generates more $^\bullet$OH radicals under the visible light illumination. This is further confirmed by the terephthalic acid (TA) probe experiment. This experiment also confirms the generation of hydroxyl radicals during photocatalytic reaction.[49] It is well-known that the $^\bullet$OH radicals react with TA to yield

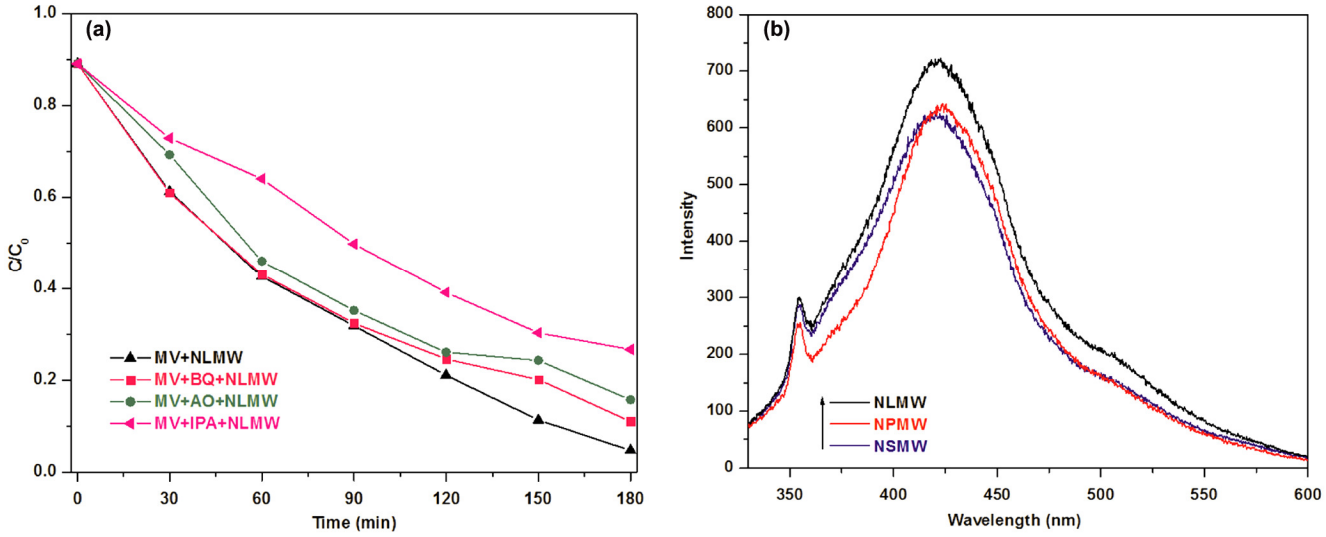

Fig. 5 – (a) Photodegradation of MV over NLMW in the presence of scavengers. (b) Fluorescence spectra of visible light irradiated photocatalysts (NLMW, NSMW, and NPMW) suspension in 2 mM terephthalic acid for 180 min of irradiation time.

2-hydroxy terephthalic acid (TAOH) which emits a unique fluorescence signal at 425 nm. Therefore, herein, the formation of TAOH as a result of photocatalytic hydroxylation of TA in the presence of catalyst was used as evidence for the production of $^{\bullet}$OH radicals. The fluorescence spectra of visible light irradiated NLMW, NPMW and NSMW suspensions in 3 mM terephthalic acid after 180 min are shown in Fig. 5b. The higher fluorescence intensity of NLMW at 425 nm as compared to that of NPMW and NSMW indicates the generation of larger number of $^{\bullet}$OH radicals for NLMW as compared to that for NPMW and NSMW under identical photocatalytic reaction conditions.

Since reusability and stability are the most important aspects for evaluating the practical and commercial applications of a catalyst, MV degradation cycling experiments were carried out in the presence of NLMW NPMW and NSMW (Supplementary Data, Fig. S6). It was observed that the extent of the degradation in every cycle is almost the same. Further, the powder XRD pattern of NLMWO, recorded after third cycle of photodegradation, remains unchanged, indicating its chemical stability (Supplementary Data, Fig. S7). Thus, the catalysts NLMW NPMW and NSMW retain their activity at least up to three cycles and may be considered attractive photocatalysts for degradation of organic contaminants.

Conclusions

All the compounds investigated herein were prepared by ethylene glycol assisted gel-burning method and characterized by powder XRD, SEM-EDS, FT-IR, UV-vis DRS and photoluminescence spectra. The powder XRD patterns and the Rietveld structural analysis revealed that all the samples crystallize in monoclinic system with $P2_1(4)$ space group. The absorption edges of these materials were observed in the visible region. The band gap energies of NLMW, NPMW and NSMW were found to be 2.47, 2.76 and 3.1 eV respectively. The color points, (x_d, y_d), values for NPMW and NSMW are (0.439, 0.554) and (0.448, 0.544), respectively. The CIE color purity for the NPMW and NSMW are calculated as 94% and 95.9% respectively. Photocatalytic studies show the dye (MV) degradation to be about 91%, 80% and 78% after 180 min visible light illumination respectively in the presence of NLMW, NPMW and NSMW. The relatively high photocatalytic activity of NLMW can be attributed to its lower band gap energy. Quenching studies confirm that $^{\bullet}$OH radicals play a major role in the dye degradation process. From the cyclic runs, NLMW NPMW and NSMW catalysts are found to be stable and retain their catalytic activity up to three cycles, and hence, may be considered as attractive photocatalysts for degradation of organic contaminants.

Supplementary Data

Supplementary data associated with this article are available in the electronic form at http://www.niscair.res.in/jinfo/ijca/IJCA_57A(03)435-443_SupplData.pdf.

Acknowledgement

The authors would like to acknowledge the University Grants Commission (UGC), New Delhi, India, under UPE-FAR (14-5/2012 (NS/PE)) programme and Council of Scientific & Industrial Research (CSIR), New Delhi, India, under the CSIR-scheme (No. 01(2857)/16/EMR-II) for financial support. MV thanks the UGC for the award of BSR fellowship (F. 18-1/2011(BSR)).

References

1 Banat I M, Nigam P, Singh D & Marchant R, *Bioresour Technol*, 58 (1996) 217.
2 Kunz A, Zamora P P, Moraes S G & Duran N, *Q Nova*, 25 (2002) 78.
3 Nascimento C, de Paiva Magalhaes D, Brandao M, Santos A B, Chame M, Baptista D, Nishikawa M & da Silva M, *Braz Arch Biol Technol*, 54 (2011) 621.
4 Saber O, Alomair H, Abu-Abdeen M D & Aljaafari A, Fast *Acta Metall Sin (Eng. Lett)*, https://doi.org/10.1007/s40195-017-0682-4 (2017).
5 Seddigi Z S, *Bull Environ Contam Toxicol*, 84 (2010) 564.
6 Rauf M A & Ashraf S S, *J Hazard Mater*, 166 (2009) 6.
7 Grzechulska J & Morawski A W, *Appl Catal, B: Environ*, 36 (2002) 45.
8 Kubacka A, Garcia M F & Colon G, *Chem Rev*, 112 (2012) 1555.
9 Gaya U I & Abdullah A H, *J Photochem Photobiol C: Photochem Rev*, 9 (2008) 1.
10 Mills A & Hunte S L, *J Photochem Photobiol A: Chem*, 108 (1997) 1.
11 Zhang Q, Cagin T & Goddard III W A, *Proc Natl Acad Sci USA*, 103 (2006) 14695.
12 Huang Q, Santoro A, Lynn J W, Erwin R W, Borchers J A, Peng J L, Ghosh K & Greene R L, *Phys Rev B*, 58 (1998) 2684.
13 Koster G, Klein L, Siemons W, Rijnders G, Dodge J S, Eom C B, Blank D H A & Beasley M R, *Rev Mod Phys*, 84 (2012) 253.
14 Staruch M, Violette D & Jain M, *Mater Chem Phys*, 139 (2013) 897.
15 Guo R, Cross L E, Park S E, Noheda B, Cox D E & Shirane G, *Phys Rev Lett*, 84 (2000) 5423.

16 Nagata Y, Suzuki N, Uchida T, Mosley W D, Klavins P & Shelton R N, *Physica C: Supercond*, 195 (1992) 195.
17 King G, Thimmaiah S, Dwivedi A & Woodward P M, *Chem Mater*, 19 (2007) 6451.
18 King G & Woodward P M, *J Mater Chem*, 20 (2010) 5785.
19 Anderson M T, Greenwood K B, Taylor G A & Poeppelmeier K R, *Prog Solid State Chem*, 22 (1993) 197.
20 Lufaso M W, Barnes P W & Woodward P M, *Acta Crystallogr Sect B: Struct Sci*, 62 (2006) 397.
21 Millange F, Caignaert V, Domenges B & Raveau B, *Chem Mater*, 10 (1998) 1974.
22 Woodward P M, Suard E & Karen P, *Am Chem Soc*, 125 (2003) 8889.
23 Sekiya T, Yamamoto T & Torii Y, *Bull Chem Soc Japan*, 57 (1984) 1859.
24 Lopez M L, Veiga M L & Pico C, *J Mater Chem*, 4 (1994) 547.
25 Arillo M A, Gomez J, Lopez M L, Pico C & Veiga M L, *Solid State Ionics*, 95 (1997) 241.
26 Tarvin R & Davies P K, *J Am Ceram Soc*, 87 (2004) 859.
27 Arillo M A, Gomez J, Lopez M L, Pico C & Veiga M L, *J Mater Chem*, 7 (1997) 801.
28 Knapp M C & Woodward P M, *J Solid State Chem*, 179 (2006) 1076.
29 Feraru S, Borhan A I, Samoila P, Mita C, Cucu-Man S, Iordan A R & Palamaru M N, *J Photochem Photobiol A*, 307 (2015) 1.
30 Iwakura H, Einaga H & Teraoka Y, *J Nov Carb Resor Sci*, 3 (2011) 1.
31 King G, Wayman L M & Woodward P M, *J Solid State Chem*, 182 (2009) 1319.
32 Hou J, Yin X, Huang F & Jiang W, *Mater Res Bull*, 47 (2012) 1295.
33 Sreenu K, Naveen Kumar V, Reddy J R, Sudhakar Reddy C H & Vithal M, *J Mater Sci Mater Electron*, 27 (2016) 4194.
34 Naveen Kumar V, Ravi G, Reddy J R, Suresh P, Muniratnam N R & Vithal M, *J Am Ceram Soc*, 97 (2014) 1829.
35 Blasse G, Van Den & Heuvel G P M, *J Solid State Chem*, 10 (1974) 206.
36 Malathi M, Sreenu K, Ravi G, Kumar P V, Sudhakar Reddy C H, Ravinder G, Radha V & Vithal M, *J Chem Sci*, 129 (2017) 1193.
37 Sharits A R, Khoury J F, Woodward P M, *Inorg Chem*, 55 (2016) 12383.
38 Birkel Denault A K, George N C & Seshadri R, *Mater Matter*, 7 (2012) 22.
39 Chen L, Lin C C, Yeh C W & Liu R S, *Materials*, 3 (2010) 2172.
40 Liu Q, Li X, Zhang B, Wang L, Zhang Q & Zhang L, *Ceram Int*, 42 (2016) 15294.
41 Liu Q, Shen J, Tian X, Lixi W, Zhang J, Zhang Q & Zhang L, *Ceram Int*, 42 (2016) 13855.
42 Radha V, Suresh P, Ravi G, Naveen Kumar V, Reddy J R & Vithal M, *J Rare Earth*, 33 (2015) 837.
43 Radha V, Vijaya Kumar B, Rama Devi V, Jaya Prakash D & Vithal M, *Spectroscopy Letters*, 44 (2011) 258.
44 *CIE (1932) Commission internationale de l'Eclairage Proceedings*, (Cambridge University Press, Cambridge) 1931.
45 Ravinder G, Ravi G, Reddy J R, Veldurthi N K, Sreenu K & Vithal M, *Photochem Photobiol*, 92 (2016) 223.
46 Breault T M & Bartlett B M, *J Phys Chem C*, 117 (2013) 8611.
47 Hislop K A & Bolton J R, *Environ Sci Technol*, 33 (1999) 3119.
48 Zhang Y, Zhang N, Tang Z R & Xu Y J, *Chem Sci*, 4 (2013) 1820.
49 Ishibashi K, Fujishima A, Watanabe T & Hashimoto K, *Electrochem Commun*, 2 (2000) 207.